Materials Research Express

PAPER • **OPEN ACCESS**

Superconductivity of superhydride CeH_{10} under high pressure

Materials Research Express

PAPER

Superconductivity of superhydride CeH_{10} under high pressure

Prutthipong Tsuppayakorn-aek[1,2], **Udomsilp Pinsook**[1,2], **Wei Luo**[3], **Rajeev Ahuja**[3,4] and **Thiti Bovornratanaraks**[1,2]

[1] Extreme Conditions Physics Research Laboratory (ECPRL) and Physics of Energy Materials Research Unit (PEMRU), Department of Physics, Faculty of Science, Chulalongkorn University, Bangkok 10330, Thailand
[2] Thailand Center of Excellence in Physics, Ministry of Higher Education, Science, Research and Innovation, 328 Si Ayutthaya Road, Bangkok 10400, Thailand
[3] Condensed Matter Theory Group, Department of Physics and Materials Science, Uppsala University, Box 530, SE-751 21 Uppsala, Sweden
[4] Applied Materials Physics, Department of Materials and Engineering, Royal Institute of Technology (KTH), S-100 44 Stockholm, Sweden

E-mail: Udomsilp.P@Chula.ac.th

Keywords: superconductor, high pressure, cerium hydride

OPEN ACCESS

RECEIVED
10 June 2020

REVISED
30 July 2020

ACCEPTED FOR PUBLICATION
3 August 2020

PUBLISHED
12 August 2020

Abstract

A large class of metal superhydrides was found to be a conventional BCS superconductor under high pressures. In this work, we focused on cerium decahydride, CeH_{10}. Ce is a member of the so–called lability belt in the periodic table, where the physical properties can be largely affected by pressure. It was reported and we confirmed that CeH_{10} can be formed with the Fm-3m structure, where a cerium atom is embedded in a H_{32} clathrate cage. Our phonon calculations show that it is dynamically stable at around 300 GPa onwards. We examined the evolution under pressures of the phonons, the electronic states, the Fermi surface, and the electron localization function (ELF). There exists a small van Hove singularity (vHs), and it gradually moves to below the Fermi surface as pressure increases. This behaviour associating with the reducing value of the electron-phonon coupling strength (λ), causes the superconductivity transition temperature (T_c) to gradually reduce under pressures. The maximum T_c is 45 K at 300 GPa.

Introduction

Metal polyhydrides have attracted large attention from condensed matter research community as they become a metal and possibly a conventional Bardeen–Cooper–Schrieffer (BCS) based superconductor with a high value of transition temperature (Tc) under pressure [1–13]. From the theoretical consideration, there were several theoretical surveys led by Peng *et al* [14] Semenok *et al* [15] Zurek and Bi [16], and Pinsook [17]. They gave a comprehensive overview of the current achievement on the structural prediction of polyhydrides and their superconducting properties at high pressures. Among large number of predicted structures, there is a noticeably large class of metal decahydrides, MH_{10}, where M = Sr, K, Y, La, Ac, Ce, Th, etc Most of these MH_{10} share a common Fm-3m structure, which can be viewed as a clathrate structure. In this structure, hydrogen atoms form a H_{32} cage which hosts a metal atom inside. Surprisingly, most of the metals that form MH_{10} belongs to the so–called lability belt, i.e. d^0 and d^1 belts in the periodic table. Furthermore, there are several members of this class that exhibit Tc > 273 K from theoretical calculations, i.e. LaH_{10} (Tc = 274–286 K at 210 GPa) and YH_{10} (T_c = 305–326 K at 250 GPa) [13]. The existence of LaH_{10} has been confirmed by experiment at 180–200 GPa with Tc around 260 K [18]. Another theoretical prediction on the Th–H system revealed the existence of ThH_{10} with an Fm-3m structure [19], and it was predicted that T_c = 220–241 K at 100 GPa. The Fm-3m–ThH_{10} was confirmed by experimental observation, and it was shown that T_c = 159–161 K at 170–175 GPa [20]. The YH_x compounds have been synthesized [21]. The existence of YH_6 and YH_9 have been confirmed with T_c = 227 K at 237 GPa and T_c = 243 K at 201 GPa, respectively. However, YH_{10} has not yet been found up to 237 GPa [21].

By comparison with LaH_{10}, we are particularly interested in CeH_{10} because Ce shares some similarity with La. For example, they have similar 3^+ ionic radii and similar atomic masses. However, Ce has two oxidation

states, i.e. 3^+ and 4^+. The 4^+ ionic radius of the Ce atom is quite smaller as Ce has the [Xe] $4f^1 5d^1 6s^2$ electronic configuration, whereas La has the [Xe] $5d^1 6s^2$ electronic configuration. The discrepancy between trivalent and tetravalent metals would manifest in their different bondings under pressure. In addition, there will be some complication from the strong correlation of the f–electron. Recently, there has been a theoretical prediction on the existence of CeH_{10} led by Peng *et al* [14] and Li *et al* [11]. By considering the structural convex hull, Peng *et al* predicted that the CeH_{10} compound can be formed at 200 GPa with either Fm-3m or R-3m structure [14]. The R-3m structure can be viewed as a distorted Fm-3m structure as well. On the experimental side, the CeH_x compounds have been synthesized by Salke *et al* [22] using a laser–heated diamond anvil cell (DAC). Their compounds can be identified as CeH_2, CeH_3 and CeH_9 phases at different pressures by using synchrotron x–ray diffraction (XRD). The structure of CeH_9 was identified as a hexagonal clathrate structure with the $P6_3/mmc$ space group at 80 GPa. We refer to this phase as hcp–CeH_9 from now on. Its T_c has not been measured but it was estimated to be around 117 K at 200 GPa [22]. The existence of hcp-CeH_9 has been confirmed by another independent experiment by Li *et al* [23] Salke *et al* [22] also searched for CeH_{10} up to 200 GPa, but they did not succeed.

In this work, we have followed the theoretical work of Peng *et al* [14] and extended our investigation into CeH_{10} and the evolution of its superconductivity under pressure in more detail. We have rechecked the structure searching for the possible structural deviation. Consequently, we used the DFT method to calculate the phonon dispersion, the electronic states, the Fermi surfaces, electron localization function (ELF), the electron-phonon coupling strength under pressure. The presence of the f-electron is properly taken into the account. We found that the Fm-3m phonons at 200 GPa contain some unstable modes. Thus, T_c is calculated in the pressure range of 300–700 GPa only. Surprisingly, T_c is quite low compared with that of LaH_{10}. We will discuss the cause that diminishes the electron–phonon coupling strength in CeH_{10}.

Computational details

All of the density functional calculations in this work used the generalized gradient approximation of the Perdew–Burke–Ernzerhof (GGA-PBE) functional [24] for the exchange-correlation functional. We employed the projector augmented wave (PAW) method [25], as implemented in the Vienna *ab initio* simulation package (VASP) [26]. The PAW potentials with 12 valence electrons ($5s^2 5p^6 4f^1 5d^1 6s^2$) for Ce and 1 valence electron (s^1) for H were applied with a plane wave basis set up to a cutoff energy of 700 eV and a $10 \times 10 \times 10$ k-point mesh generated by the Monkhorst–Pack (MP) method [27]. The core radii of Ce and H are 2.57 Bohr and 0.80 Bohr, respectively, which are small enough that the overlap of spheres will not occur under applied pressure. All of the structural parameters are fully relaxed by using the Methfessel–Paxton smearing method [26] and the conjugate gradient scheme. All considered structures were relaxed at each pressure until the Hellman–Feynman forces became less than 10^{-3} eV Å^{-1}. The phonon calculations were calculated by using the *ab initio* lattice dynamics with the finite displacement method, as implemented in the VASP code together with the PHONOPY package [28]. For the superconducting phase, we calculated the electron–phonon coupling (EPC) within the density functional perturbation theory [29] via Quantum Espresso (QE) package [30]. In order to compare the QE results with those of VASP, a compatible PAW potentials with 12 valence electrons ($5s^2 5p^6 4f^1 d^1 6s^2$) for Ce [31] and 1 electron (s^1) for H have also been employed in QE. The plane-wave energy cutoff of 60 Ry was used. The Brillouin zone (BZ) integrations in the electronic and phonon calculations were performed using the MP meshes. The EPC matrix elements were computed in the first BZ on $4 \times 4 \times 4$ q-meshes using individual EPC matrices obtained with a $24 \times 24 \times 24$ k-points mesh. The Allen-Dynes equation [32] was used with the effective Coulomb pseudopotential parameter, $\mu^* = 0.10$ and 0.13, as follows;

$$T_c = \frac{\omega_{\log}}{1.2} \exp\left[-\frac{1.04(1+\lambda)}{\lambda - \mu^*(1+0.62\lambda)}\right], \quad (1)$$

where $\omega_{\log}$ is the logarithmic average of the spectral function. λ is the total electron-phonon coupling strength. We found that $\lambda < 1.5$ in most of our cases, thus this form of Allen-Dynes equation is quite sufficient.

Results and discussion

We have independently searched for the predicted phase of CeH_{10} by using several structure searching methods [33, 34]. These methods give the same Fm-3m structure for CeH_{10}. Thus, we proceeded further to the calculation of its superconductivity and the associating Tc. Figure 1(a) illustrates the Fm-3m structure, where H atoms form an H_{32} clathrate cage which hosts a Ce atom inside. The H_{32} clathrate cage is shown in figure 1(b). The polygon faces of the H_{32} clathrate cage contain six squares and twelve hexagons (the [$4^6 6^{12}$] polyhedron). We shall refer to this phase as fcc-CeH_{10} from now on. This phase is in good agreement with the structure of

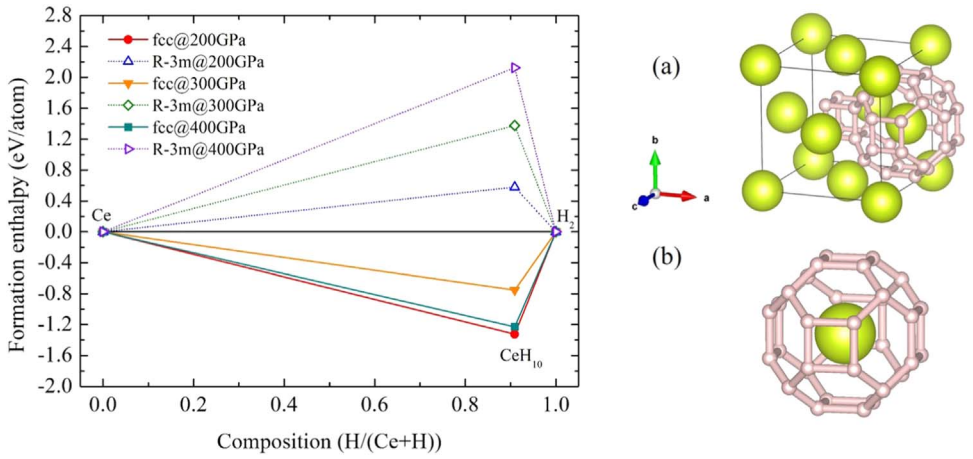

Figure 1. Left: the formation enthalpy per atom of CeH_{10} is presented in the form of convex hulls. Right: the crystal structure of fcc-CeH_{10}. (a) The Fm-3m structure. (b) The H_{32} clathrate cage with six square and twelve hexagonal ($[4^6 6^{12}]$) faces and the Ce atom (draw by VESTA [35]).

CeH_{10} predicted by Li *et al* [11] and Peng *et al* [14]. We calculated the formation enthalpy of fcc-CeH_{10} compared with the H_{32} structure and fcc-Ce. We found that fcc-CeH_{10} can be formed at approximately 40 GPa. Peng *et al* [14] used convex hull calculation to show that fcc-CeH_{10} can be formed at 200 GPa.

As mentioned earlier, the R-3m structure can be considered as a distorted Fm-3m structure. Thus, we also compared the structural stability between the R-3m and Fm-3m structures. The convex hulls showed that the Fm-3m structure is more thermodynamically stable between 200–400 GPa. On the other hand, the convex hulls pointed out that the R-3m structure is likely to be a metastable structure, as shown in figure 1(left).

Next, we calculated the phonon dispersion in the pressure range of 200–700 GPa by using PHONOPY [28] associated with VASP [26]. At 200 GPa, we found that the phonon calculation produces some imaginary numbers, instead of finite frequencies, in some of the optical modes around the Γ-point, as shown in figure 2(a). These imaginary modes indicate that the fcc-CeH_{10} structure is dynamically unstable. At this pressure, the highest phonon frequencies are around 62 THz. At 300 GPa, the imaginary frequencies disappear. In fact, the previously unstable optical modes have finite frequencies of 7.39 and 9.17 THz at the Γ-point. Even though, the convex hull suggested that fcc-CeH_{10} can be formed from 200 GPa onward [14], we suggest here that it can only be dynamically stable from 300 GPa. This is in agreement with experimental finding that CeH_{10} has not been found up to 200 GPa [22]. It is worth noticing here that the vibrations of the Ce atom are dominated at the low frequency region, i.e. <10 THz, whereas the vibrations of the H_{32} cage are dominated in the high frequency region, i.e. >20 THz. There is a large frequency gap due to the large difference between the masses of Ce and H, and the coupling between the two constituent species. The highest phonon frequencies are around 76 THz at this pressure. At the pressure range of 300–700 GPa, the phonons are all stable. Generally, the phonon frequencies increase as pressure increases. The frequency gap between the low and high frequency regions still remains.

At this stage, we discuss the electronic states. The calculated electronic band structure and projected density of state (PDOS) of fcc-CeH_{10} at pressure 400 and 700 GPa are shown in figures 3(a)–(d). The electronic states have some variation under pressure, hence we chose 400 GPa as the center of our discussion. From figure 3, the PDOS exhibits significant contribution from the f-electrons at Fermi energy (E_f) under high pressure. The PDOS also indicates that fcc-CeH_{10} is a metal with quite low density of states at E_f, i.e. 0.22 states/eV. This is because all of the energy bands cross the Fermi energy with steep slope. In the other words, there is no flat dispersion near the E_f. In fcc-LaH_{10} [13, 36] and hcp-CeH_9 [22], the density of states at E_f is quite large due to some flat bands in the former and shallow-slope bands in the latter. There is a small expression of the van Hove singularity (vHs) at the E_f at 400 GPa, marked by an arrow in figure 3(c), but it gradually moves down to lower energy as pressure increases. At 700 GPa, the position of the vHs is a little below E_f, as marked by an arrow in figure 3(d). This makes the density of states at E_f even lower at higher pressure. Table 1 gives a summary on the number of states (N_f) at E_f of fcc-CeH_{10} comparing with the other related structures.

At around the Γ-point close to E_f, the band dispersions are dominated by the weaving of the up-running bands from below E_f and down-running bands above E_f. When up- and down-running bands cross each other with their steep slopes, there is a possibility that the dispersions around the crossing are likely to form the Dirac cones. For example, the crossing bands along the M $\rightarrow$ Γ branch are likely to form the Dirac cones. Some of

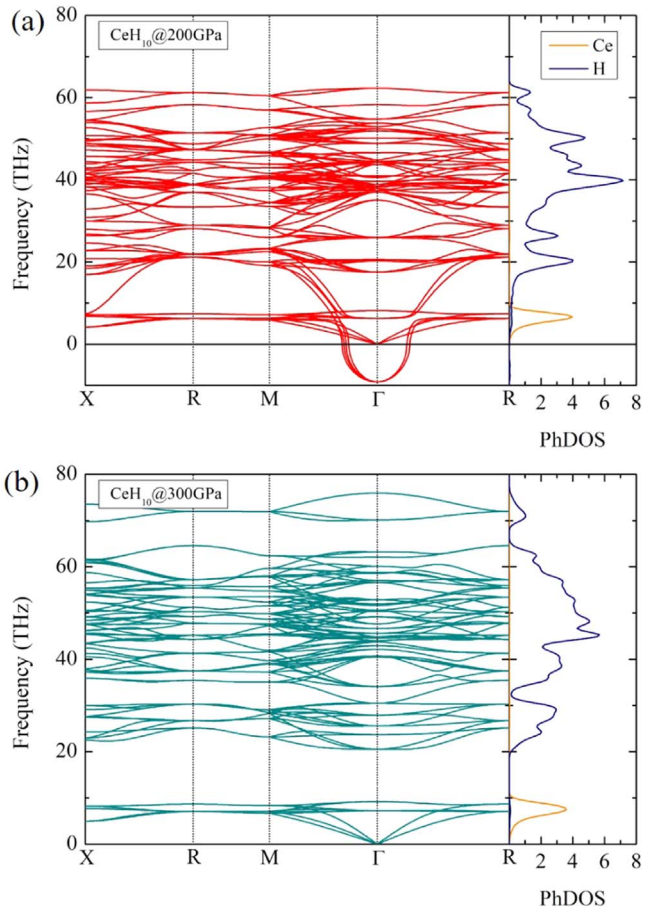

Figure 2. The phonon dispersion of fcc-CeH_{10} from PHONOPY associated with VASP at (a) 200 GPa and (b) 300 GPa.

these crossing bands along the M $\rightarrow$ Γ branch are broken at 700 GPa, as shown in the dashed circle in figure 3(b) comparing with that in figure 3(a).

As we explicitly brought the f-electron into the calculation, we would like to investigate the effect of strong correlation to the band structure as well. In order to verify this feature, we calculated the electronic band structure by including an effective Hubbard parameter, U = 4 eV, for the Ce atom (figure 4). We found that the ground states are mostly intact. The band structures around the Fermi level resemble those of the GGA calculation, except some low-lying excited states at Γ point occur at lower energy, and some of the crossing bands along the M $\rightarrow$ Γ branch are broken, as shown in the dashed circle in figure 4. Nevertheless, the states near Fermi level are similar to those of the GGA. Thus, the strong correlation of the f-electron should have minimum impact on the superconductivity.

From the band structure, we can construct the Fermi surfaces of fcc-CeH_{10}. The associated Fermi surface (FS) at 400 GPa are shown in figure 5. The surface #1–#3 are from the down-running dispersion around the Γ-point with steep slopes. Thus, these surfaces are just small polyhedral objects in the larger Brillouin zone. They contribute almost nothing to the superconductivity. The most important contribution to the superconductivity of fcc-CeH_{10} is from the surface #4–#5. In fact, the surface #4–#5 are very special. They come from the accidental crossing between the up- and down- running dispersions at exactly the Fermi energy along the Γ $\rightarrow$ X, Γ $\rightarrow$ M and Γ $\rightarrow$ R branches for the surface #4, and along Γ $\rightarrow$ X $\rightarrow$ M $\rightarrow$ Γ branches for the surface #5. Consequently, there could be a large number of the Dirac cones at the band crossing. For example, there are 2 cones for each Γ $\rightarrow$ X $\rightarrow$ M $\rightarrow$ Γ branch, and there are 12 equivalent Γ $\rightarrow$ X $\rightarrow$ M $\rightarrow$ Γ branches in the Brillouin zone. Therefore, there are 24 Dirac cones associating with the surface #5. Furthermore, the shapes of the surface #4–#5 contain several parts that are parallel to each other, i.e. these parts can be connected by a common nesting vector. These are the so-called Fermi surface nesting, see [37] for example. Thus, the surface #4–#5 take an important role in the superconductivity of fcc-CeH_{10}. The surface #6 is in the form of small pockets which are barely connected to each other, and hence gives insignificant contribution to the superconductivity. The Fermi surfaces have a little variation under pressure.

In order to understand the nature of bonding of fcc-CeH_{10}, we analyze the electron localization function (ELF) [39] in the (001) plane, as shown in figure 6. The ELF was a useful tool to study the bondings in many

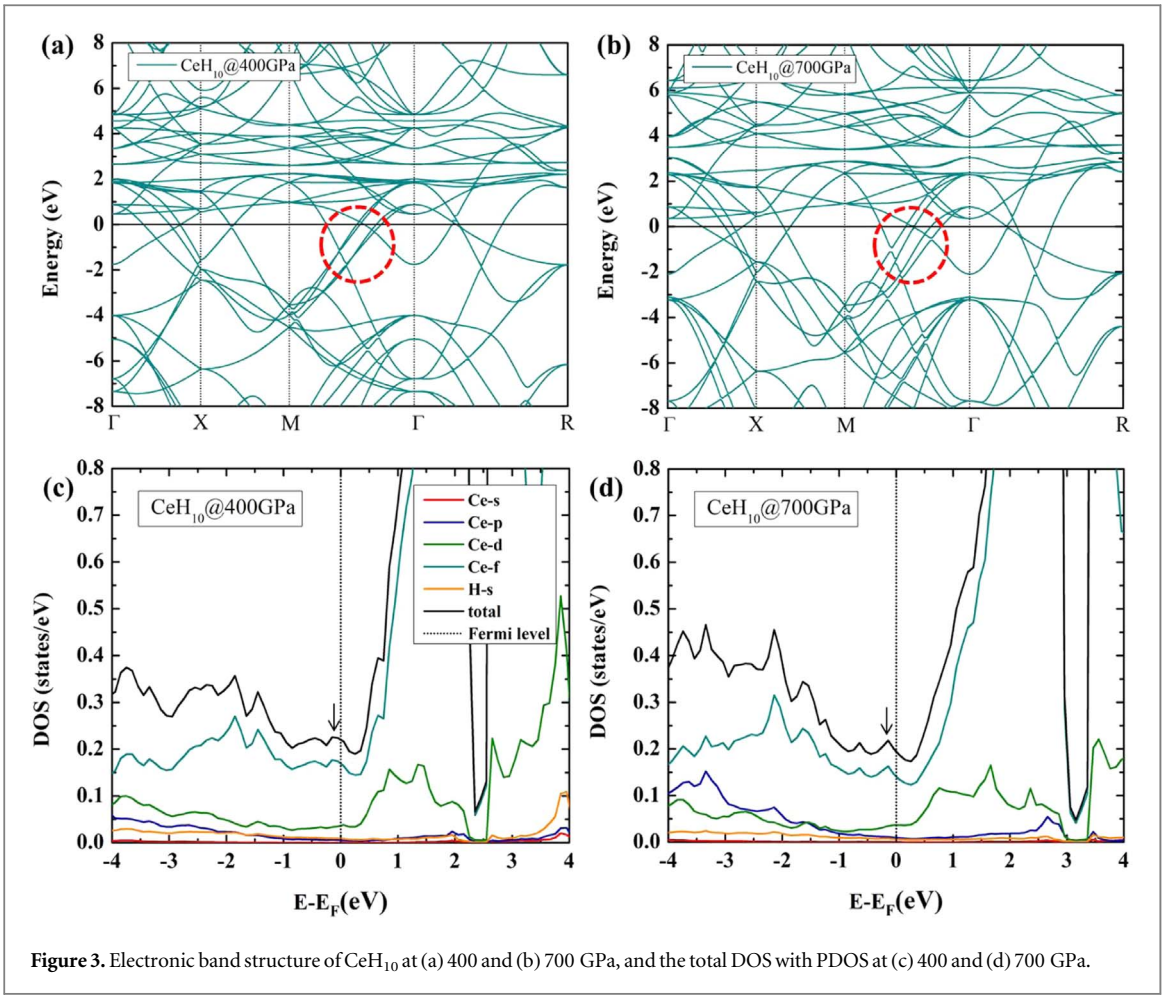

Figure 3. Electronic band structure of CeH_{10} at (a) 400 and (b) 700 GPa, and the total DOS with PDOS at (c) 400 and (d) 700 GPa.

Table 1. The calculated parameters and T_c of fcc–CeH_{10}, compared with those of fcc– LaH_{10} [13, 36] and hcp–CeH_9 [22].

Metal hydrides	Pressure (GPa)	N_f(states/eV)	λ	ω_{log} (K)	T_c (K)
fcc–LaH_{10}[a]	210	0.73	3.41	848	238
fcc–LaH_{10}[b]	300	0.95	2.20	—	220
hcp–CeH_9[c]	200	0.73	2.30	740	117
fcc–CeH_{10}[d]	300	0.22	0.64	1632	45

[a] Refereence [13].
[b] Refereence [36].
[c] Refereence [22].
[d] This work.

metals and compounds, such as Li [40], S [41] c and XeC [42]. At 0 GPa, the ELF shows no structured bonding, and most electrons are localized around the Ce atoms, as shown in figure 6(a). At 100 GPa, the H_{32} cage is formed, but there is only weak interaction with the Ce atom, as shown in figure 6(b). There are several areas that have low electron population. Furthermore, the H_1–H_2 bonding seems to be weakly formed. At 100–200 GPa, there were reports on the so-called atomic-like states in hcp-CeH_9 [22, 23], and fcc-LaH_{10} [13, 18]. This is not the case for fcc-CeH_{10}. At 400 GPa, the H_{32} cage forms more structured bondings with the Ce atom, as shown in figure 6(c). The H_1–H_2 bonding seems to be more strongly established. However, the H_1–H_2 bond length is very short, i.e. 1.109 Å, only. This also approaches the atomic hydrogen limit. It is worth noting here that H–H cannot be too close as the quantum nucleus effect will be likely to keep them apart [43]. This would be a subject of future investigation.

Finally, we calculated the superconductivity of fcc-CeH_{10}, starting from calculating the central feature, i.e. the spectral function, α^2F by using QE [29, 30]. The spectral function at 300 GPa is shown as a solid line in figure 7(a). The spectral function can be clearly divided into two parts, i.e. the heavier Ce atom and the lighter H_{32} cage parts. From figure 7(a), the accumulated λ is shown as a dashed line. It reflects the strength of the

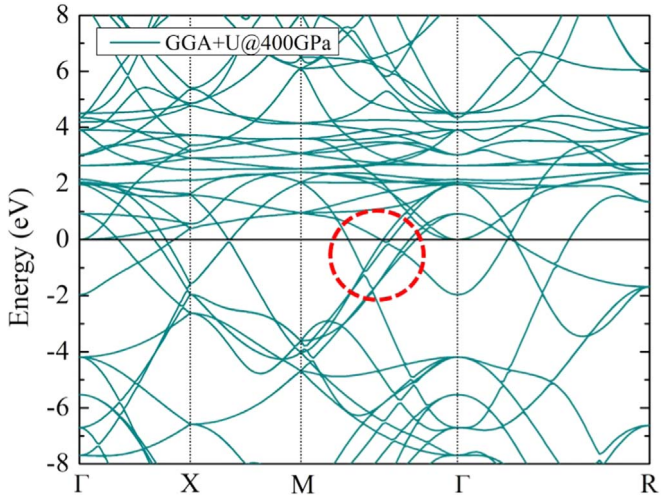

Figure 4. Electronic band structure of CeH_{10} is calculated by using GGA + U (U = 4 eV) at 400 GPa.

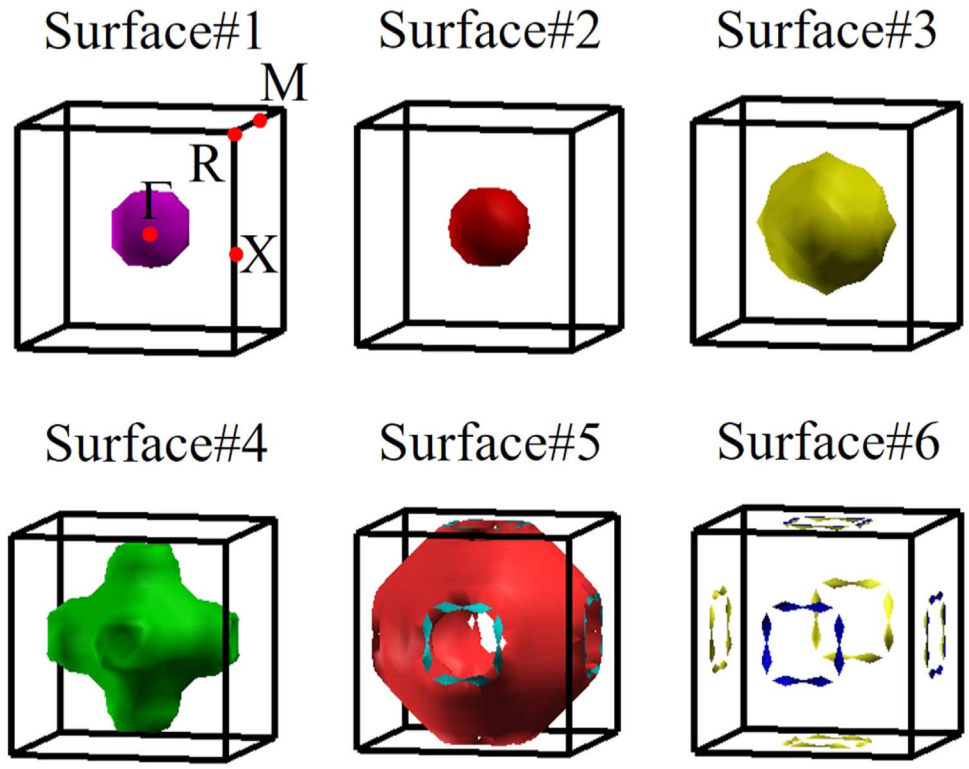

Figure 5. Fermi surface of CeH_{10} at 400 GPa (draw by XCrySDen [38]).

electron-phonon coupling (EPC) in each region of the phonon frequencies. The contribution of λ in the lower frequency region from the heavier Ce atom is about 0.09, whereas the contribution of λ the higher frequency region from the H_{32} cage is about 0.55. The total λ is 0.64 at 300 GPa. In hcp-CeH_9 at 200 GPa, the contributions of λ are about 0.6 and 1.7 from the Ce atom and the H cage, respectively [22]. In fcc-LaH_{10} at 300 GPa, the contributions of λ are about 0.4 and 1.8 from the La atom and the H cage, respectively [36]. By using Hopfield analysis [44, 45], the electron-phonon coupling strength parameter can be expressed as,

$$\lambda \approx \frac{N_f I^2}{M\omega_2^2}, \tag{2}$$

where I^2 is the average strength of the electron-phonon interaction, N_f is the density of states at the Fermi level, M is the characteristic mass of the system, and ω_2 is the characteristic frequency of the system. As discussed

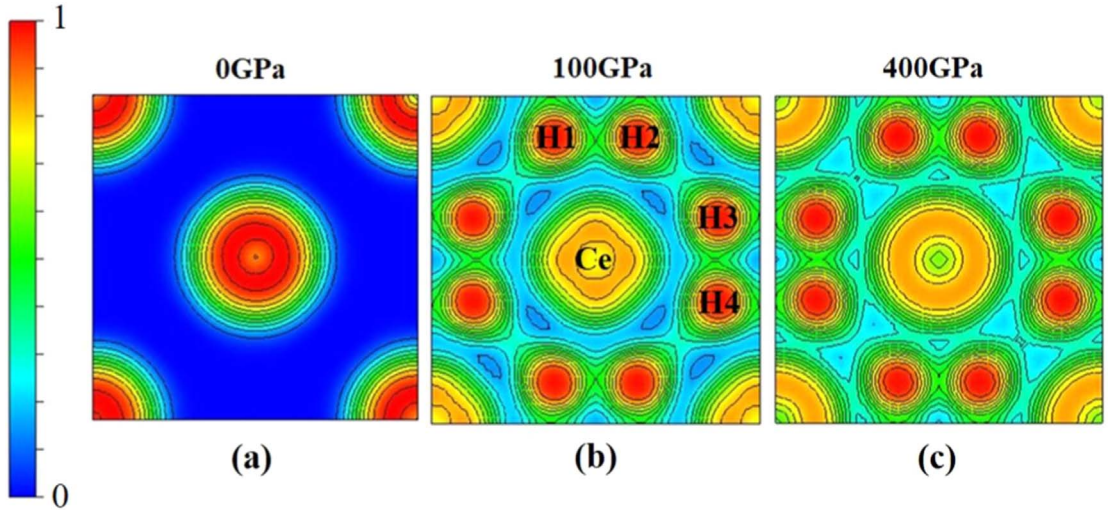

Figure 6. The electron localization function (ELF) in the (001) atomic plane of the CeH_{10} framework under pressures of 0, 100, and 400 GPa (draw by VESTA [35]).

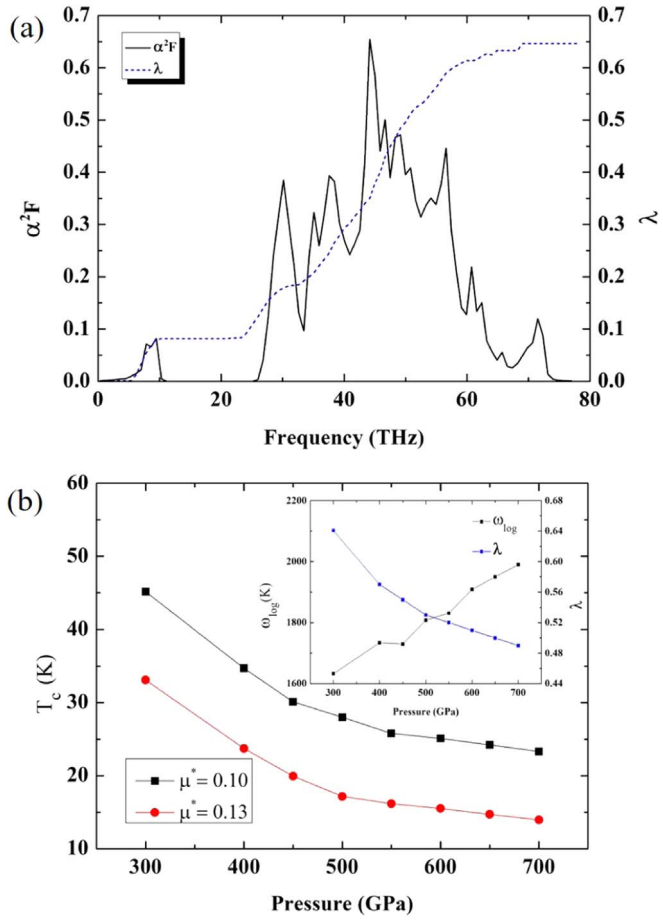

Figure 7. (a) The spectral function α^2F (solid line) and the accumulated λ (dashed line) as a function of frequency of fcc-Ce_{10} at 300 GPa. (b) Critical temperature as a function of pressure with $\mu^* = 0.10$ (black line) and 0.13 (red line). λ (blue squares) and ω_{log} (black squares) as a function of pressure are shown in the inset.

earlier, we found that there can be the Fermi surface nesting in the surface #4–#5, which could give rise to a significant value of I^2. Disappointedly, we also found from table 1 that N_f is comparatively much lower in fcc-CeH_{10} due to the steep slope of the energy dispersion close to E_f. This is in contrast with hcp-CeH_9 where the dispersion close to E_f is quite shallow [22], and with fcc-LaH_{10} where there exist several flat bands close to E_f [36].

From the spectral function, the logarithmic average of the phonon frequency, ω_{log}, can also be evaluated, and it is 1,632 K for fcc-CeH_{10} at 300 GPa. In addition, we also calculated λ and ω_{log} as a function of pressure, as shown in the inset of figure 7(b). Typically, λ is a decreasing function of pressure, whereas ω_{log} is an increasing function of pressure. By using the Coulomb pseudopotential parameter $\mu^* = 0.10$ and 0.13 and equation (1), we calculated the superconducting critical temperature T_c. We found that T_c decreases monotonically between 300 and 700 GPa, as shown in figure 7(b). The maximum T_c of fcc-CeH_{10} is 45 K at 300 GPa with $\mu^* = 0.10$. This T_c is quite low compared with 117 K of hcp-CeH_9 at 200 GPa [22] and 220 K of fcc-LaH_{10} at 300 GPa [36]. This behavior is solely because of the low value of N_f and hence of λ, as they are approximately related by equation (2). All the parameters and T_c are summarized in table 1.

Conclusion

In this work, we have calculated the superconductivity of CeH_{10} under pressure by using DFT. We found that the ground state structure is the Fm-3m structure, which is a clathrate structure. The phonon calculation suggested that it is dynamically stable from 300 GPa onwards. Then, we calculated the electronic structure and reported the electronic dispersion around the Fermi level, the Fermi surface, and the electron localization function. We found that the f-electron states dominate the states at the Fermi level. However, the density of states at the Fermi level is quite low. In addition, the electronic structure suggested that CeH_{10} could be an exotic material due to some special topology in the Fermi surface. Next, we calculated the spectral function and T_c as a function of pressure. We found that CeH_{10} have low lambda compared with those of CeH_9 and LaH_{10} at similar pressures. This is due to low density of states at the Fermi level. The T_c is maximum around 45 K at 300 GPa.

Acknowledgments

We are deeply grateful for the kindness of Dr. Lorenzo Paulatto for helping us generate the cerium PAW pseudopotential for using in the quantum espresso package. We gratefully acknowledge NSC (National Computer Center, Linköping, Sweden) in Sweden for providing computing time. This research is supported by Ratchadapisek Somphot Fund for Postdoctoral Fellowship, Chulalongkorn University. This work has been partially supported by Sci Super-IV research grant, Faculty of Science, Chulalongkorn University. T B acknowledge Thailand Research Fund contract number RSA5880058. This research is funded by Chulalongkorn University; Grant for Research. R A and W L thank the Swedish Research Council and Swedish Research Links for financial support.

ORCID iDs

Udomsilp Pinsook https://orcid.org/0000-0002-8450-7751
Rajeev Ahuja https://orcid.org/0000-0003-1231-9994
Thiti Bovornratanaraks https://orcid.org/0000-0001-6943-4032

References

[1] Cui W, Bi T, Shi J, Li Y, Liu H, Zurek E and Hemley R J 2020 Route to high-Tc superconductivity via CH4-intercalated H3S hydride perovskites *Phys. Rev.* B **101** 134504
[2] Ye X, Zarifi N, Zurek E, Hoffmann R and Ashcroft N W 2018 High hydrides of scandium under pressure: potential superconductors *J. Phys. Chem.* C **122** 6298–309
[3] Bi T, Miller D P, Shamp A and Zurek E 2017 Superconducting phases of phosphorus hydride under pressure: stabilization by mobile molecular hydrogen *Angew. Chem. Int. Ed.* **56** 10192
[4] Papaconstantopoulos D A 2017 Possible high-temperature superconductivity in hydrogenated fluorine *Novel Superconducting Materials* **3** 14–22
[5] Majumdar A, Tse J S, Wu M and Yao Y 2017 Superconductivity in FeH_5 *Phys. Rev.* B **96** 201107
[6] Majumdar A, Tse J S and Yao Y 2017 Modulated structure calculated for superconducting hydrogen sulfide *Angew. Chem. Int. Ed.* **56** 11390–3
[7] Majumdar A, Tse J S and Yao Y 2019 Mechanism for the structural transformation to the modulated superconducting phase of compressed hydrogen sulfide *Sci. Rep.* **9** 5023
[8] Li Y, Hao J, Liu H, Li Y and Ma Y 2014 The metallization and superconductivity of dense hydrogen sulfide *J. Chem. Phys.* **140** 174712
[9] Zhong X, Wang H, Zhang J, Liu H, Zhang S, Song H F, Yang G, Zhang L and Ma Y 2016 Tellurium hydrides at high pressures: high-temperature superconductors *Phys. Rev. Lett.* **116** 057002
[10] Feng X, Zhang J, Gao G, Liu H and Wang H 2015 Compressed sodalite-like MgH_6 as a potential high-temperature superconductor *RSC Adv.* **5** 59292–6
[11] Li B, Miao Z, Ti L, Liu S, Chen J, Shi Z and Gregoryanz E 2019 Predicted high-temperature superconductivity in cerium hydrides at high pressures *J. Appl. Phys.* **126** 235901

[12] Errea I, Calandra M, Pickard C J, Nelson J, Needs R J, Li Y, Liu H, Zhang Y, Ma Y and Mauri F 2015 High-pressure hydrogen sulfide from first principles: a strongly anharmonic phonon-mediated superconductor *Phys. Rev. Lett.* **114** 157004
[13] Liu H, Naumov I I, Hoffmann R, Ashcroft N W and Hemley R J 2017 Potential high-Tc superconducting lanthanum and yttrium hydrides at high pressure *Proc. Natl Acad. Sci.* **114** 6990–5
[14] Peng F, Sun Y, Pickard C J, Needs R J, Wu Q and Ma Y 2017 Hydrogen clathrate structures in rare earth hydrides at high pressures: possible route to room-temperature superconductivity *Phys. Rev. Lett.* **119** 107001
[15] Semenok D V, Kvashnin A G, Kruglov I A and Oganov A R 2018 Actinium hydrides AcH_{10}, AcH_{12}, and AcH_{16} as high-temperature conventional superconductors *The Journal of Physical Chemistry Letters* **9** 1920–6
[16] Zurek E and Bi T 2019 High-temperature superconductivity in alkaline and rare earth polyhydrides at high pressure: a theoretical perspective *J. Chem. Phys.* **150** 050901
[17] Pinsook U 2020 In search for near-room-temperature superconducting critical temperature of metal superhydrides under high pressure: a review *Journal of Metals, Materials and Minerals* **30** 31–41
[18] Somayazulu M, Ahart M, Mishra A K, Geballe Z M, Baldini M, Meng Y, Struzhkin V V and Hemley R J 2019 Evidence for superconductivity above 260 k in lanthanum superhydride at megabar pressures *Phys. Rev. Lett.* **122** 027001
[19] Kvashnin A G, Semenok D V, Kruglov I A, Wrona I A and Oganov A R 2018 High- temperature superconductivity in a Th–H system under pressure conditions *ACS Applied Materials & Interfaces* **10** 43809–16
[20] Semenok D V, Kvashnin A G, Ivanova A G, Svitlyk V, Fominski V Y, Sadakov A V, Sobolevskiy O A, Pudalov V M, Troyan I A and Oganov A R 2019 Superconductivity at 161K in thorium hydride ThH10: synthesis and properties *Materials Today* **33** 36–44
[21] Kong P P *et al* 2019 Superconductivity up to 243 K in yttrium hydrides under high pressure arXiv:1909.10482 [cond-mat.supr-con]
[22] Salke N P *et al* 2019 Synthesis of clathrate cerium superhydride CeH_9 at 80–100 GPa with atomic hydrogen sublattice *Nat. Commun.* **10** 4453
[23] Li X *et al* 2019 Polyhydride CeH_9 with an atomic-like hydrogen clathrate structure *Nat. Commun.* **10** 3461
[24] Perdew J P, Burke K and Ernzerhof M 1996 Generalized gradient approximation made simple *Phys. Rev. Lett.* **77** 3865–8
[25] Blöchl P E 1994 Projector augmented-wave method *Phys. Rev.* B **50** 17953–79
[26] Kresse G and Furthmü ller J 1996 Efficient iterative schemes for *ab initio* total-energy calculations using a plane-wave basis set *Phys. Rev.* B **54** 11169–86
[27] Monkhorst H J and Pack J D 1976 Special points for Brillouin-zone integrations *Phys. Rev.* B **13** 5188–92
[28] Togo A and Tanaka I 2015 First principles phonon calculations in materials science *Scr. Mater.* **108** 1–5
[29] Baroni S, de Gironcoli S, Dal Corso A and Giannozzi P 2001 Phonons and related crystal properties from density-functional perturbation theory *Rev. Mod. Phys.* **73** 515–62
[30] Giannozzi P *et al* 2009 QUANTUM ESPRESSO: a modular and open-source software project for quantum simulations of materials *J. Phys. Condens. Matter* **21** 395502
[31] Larquet C *et al* 2019 Band gap engineering from cation balance: the case of lanthanide oxysulfide nanoparticles *Chem. Mater.* **31** 5014–23
[32] Allen P B and Dynes R 1975 Transition temperature of strong-coupled superconductors reanalyzed *Phys. Rev.* B **12** 905
[33] Oganov A R and Glass C W 2006 Crystal structure prediction using *ab initio* evolutionary techniques: principles and applications *J. Chem. Phys.* **124** 244704
[34] Pickard C J and Needs R J 2011 *Ab initio* random structure searching *J. Phys. Condens. Matter* **23** 053201
[35] Momma K and Izumi F 2008 VESTA: a three-dimensional visualization system for electronic and structural analysis *J. Appl. Crystallogr.* **41** 653–8
[36] Liu L, Wang C, Yi S, Kim K W, Kim J and Cho J-H 2019 Microscopic mechanism of room-temperature superconductivity in compressed LaH_{10} *Phys. Rev.* B **99** 140501
[37] Yan X, Chen Y, Xiang S, Kuang X, Bi Y and Chen H 2016 High-temperature and high-pressure induced formation of the Laves-phase compound XeS_2 *Phys. Rev.* B **93** 214112
[38] Kokalj A 1999 XCrySDen—a new program for displaying crystalline structures and electron densities *J. Mol. Graphics Modell.* **17** 176–9
[39] Becke A D and Edgecombe K E 1990 A simple measure of electron localization in atomic and molecular systems *J. Chem. Phys.* **92** 5397–403
[40] Tsuppayakorn-aek P, Luo W, Watcharatharapong T, Ahuja R and Bovornratanaraks T 2018 Structural prediction of host-guest structure in lithium at high pressure *Sci. Rep.* **8** 5278
[41] Tsuppayakorn-aek P, Luo W, Pungtrakoon W, Chuenkingkeaw K, Kaewmaraya T, Ahuja R and Bovornratanaraks T 2018 The ideal commensurate value of Sc and the superconducting phase under high pressure *J. Appl. Phys.* **124** 225901
[42] Bovornratanaraks T, Tsuppayakorn-aek P, Luo W and Ahuja R 2019 Ground–state structure of semiconducting and superconducting phases in xenon carbides at high pressure *Sci. Rep.* **9** 2459
[43] Monacelli L, Errea I, Calandra M and Mauri F 2019 Black metal hydrogen above 360 GPa driven by proton quantum fluctuations arXiv:1912.05514 [cond-mat.mtrl-sci]
[44] Hopfield J J 1969 Angular momentum and transition-metal superconductivity *Phys. Rev.* **186** 443
[45] Quan Y, Ghosh S S and Pickett W E 2019 Compressed hydrides as metallic hydrogen superconductors *Phys. Rev.* B **100** 184505